



OPEN

Deep cognitive imaging systems enable estimation of continental-scale fire incidence from climate data

SUBJECT AREAS:

MATHEMATICS AND
COMPUTING

PROJECTION AND PREDICTION

ENGINEERING

ENVIRONMENTAL SCIENCES

Ritaban Dutta¹, Jagannath Aryal², Aruneema Das³ & Jamie B. Kirkpatrick²

¹Computational Informatics, The Commonwealth Scientific and Industrial Research Organisation (CSIRO), Hobart, Tasmania 7001, Australia, ²School of Geography and Environmental Studies, University of Tasmania, Private Bag 78, GPO, Hobart, Tasmania 7001, Australia, ³School of Engineering, University of Tasmania, Private Bag 78, GPO, Hobart, Tasmania 7001, Australia.

Received
10 May 2013Accepted
15 October 2013Published
13 November 2013

Correspondence and requests for materials should be addressed to R.D. (Ritaban.Dutta@csiro.au)

Unplanned fire is a major control on the nature of terrestrial ecosystems and causes substantial losses of life and property. Given the substantial influence of climatic conditions on fire incidence, climate change is expected to substantially change fire regimes in many parts of the world. We wished to determine whether it was possible to develop a deep neural network process for accurately estimating continental fire incidence from publicly available climate data. We show that deep recurrent Elman neural network was the best performed out of ten artificial neural networks (ANN) based cognitive imaging systems for determining the relationship between fire incidence and climate. In a decennium data experiment using this ANN we show that it is possible to develop highly accurate estimations of fire incidence from monthly climatic data surfaces. Our estimations for the continent of Australia had over 90% global accuracy and a very low level of false negatives. The technique is thus appropriate for use in estimating the spatial consequences of climate scenarios on the monthly incidence of wildfire at the landscape scale.

On every continent, except Antarctica, there are substantial areas in which wildfire is a frequent event^{1–13}. We have used Australia as a case study because the proportionate incidence, area and socioeconomic effects of wildfires are higher in Australia than in any other continental land mass¹⁴. Scenarios for climate change suggest that much of Australia will have climates more conducive to the incidence of wildfire than at present^{10,15}, a tendency already apparent from 1945 onwards¹⁶. Climatic variables have been long used to determine the potential for fire spread from ignition¹⁷. Lightning, a product of particular weather systems, is a major source of ignition over most of the continent^{18–20}. While it is not possible for fire to burn without dry fuel, severe fire weather conditions can facilitate spread over substantial fuel-free areas, such as water bodies, as burning material is carried in strong wind²¹. Fire can persist in areas with heavy dry fuel until conditions allow it to spread over low fuel zones. Thus, the relationship of fire incidence to climatic conditions is not confined to the weather that allows spread from ignition, but also weather that allows fire to persist in such places as stumps and tree hollows between weather events that allow it to run. The moistness of fuel strongly controls its flammability, this moistness being an integral of past precipitation and evaporation mediated by soil field capacity²². Therefore, in estimating the potential for fire incidence from climatic variables, longer time frames than the minute, hour or day are appropriate²³.

Our major aim in undertaking the work reported in the present paper was to develop an accurate system for estimating monthly wildfire incidence from readily available monthly average climatic conditions, in order to be able to refine our understanding of the implications of climate change for fire regimes. We chose to use cognitive imaging systems (Figure S1) to attempt to make this estimation, because these deep²⁴ machine learning processes have proven to be highly effective in a wide range of applications while being free of the restrictive assumptions of other predictive systems²⁵. Because there are many possible types of ANN, we trialled ten systems, with the facilitative aim to determine the most appropriate of these for our main purpose and to justify the effectiveness of proposed deep learning mechanism for the cognitive imaging system.

We obtained monthly data for evapotranspiration, sensible heat flux, solar irradiation, maximum temperature, soil moisture, wind speed, relative humidity and vapour pressure for the decade 2001–2010. There is a high degree of covariance among some of these variables, with the first three principal components derived from our data accounting for 95% of the variance, but this does not affect the outcomes from neural network analysis. We found that soil moisture, solar irradiation, and wind speed were the most significant contributors to the data variance.



Table 1 | Comparison of results for ten neural network systems

Different Neural Networks	Average Accuracy (%)	Average Sensitivity (%)	Average Specificity (%)	False Negative (%)	True Negative (%)
Feed Forward Back Propagation	73.67	67.61	69.14	9.66	81.24
Cascade	71.65	77.81	69.88	21.07	72.63
Multi-Layer Perception	85.61	80.44	79.13	10.15	86.05
Time Delay	88.21	87.41	89.54	7.62	83.78
Recurrent	92.77	82.22	80.91	1.96	86.43
Radial Basis Function	91.25	87.89	89.75	1.83	90.55
Elman	94.72	95.31	93.94	1.76	96.98
Probabilistic	90.35	89.57	89.04	4.27	85.09
Regression	65.27	70.79	69.52	25.86	78.15
Learning Vector Quantization	75.95	67.21	79.33	5.44	88.02

We used the months of November-February for our analyses because very few planned burns take place in Australia in late spring and summer, which is also the peak time for lightning strikes²⁰, giving us confidence that we are largely addressing climatic influence on wildfire.

Results

Elman neural networks¹¹ (Figure S2) produced the best level of explanation (Table 1). The Elman neural network is a simple recurrent neural network which was used for the deep²⁴ learning experimentations. It consists of an input layer, a hidden layer, and an output layer, resembling a three layer feed forward neural network. However, it also has a context layer. This context layer is fed with the unweighted output from the hidden layer. The Elman network then remembers these values and outputs them on the next run of the neural network. These values are then sent, using a trainable weighted connection, back into the hidden layer. Elman neural networks are very useful for estimating sequences, since they have a limited short-term memory. The high estimation accuracies achieved from the Elman neural network relate to its deep²⁴ learning architecture (including unsupervised feature extraction layer and supervised training based modelling layer), which provides state-space representation for dynamic systems and a recurrent neural equalizer.

Fire incidence was concentrated in northern Australia, although its centre of gravity typically shifted south between November and February (Figure 1). The predicted patterns were closely similar to the observed patterns (Table 2). The mean and standard error of the mean for estimation accuracy for the twelve test months were 92.19 (0.39), for sensitivity 95.09 (0.56), for specificity 94.31 (0.68), for false negatives 2.06 (0.43) and for true negatives 95.16 (0.60).

Discussion

The Elman ANN has been previously recommended for a related purpose²⁶. Its limited short term memory may be the key to its success in estimating spatial patterns of fire incidence, as the incidences themselves feed back to the probability of new incidences.

These spatial patterns were captured as physical features from the environmental gridded images. Its high degree of success in estimating fire incidence compared with previous attempts at estimation of fire over more restricted areas^{10,23,27}, may be as much related to the input time and space scales as to method, as the stochastic component in fire incidence is logically likely to decrease with larger time slices and larger pixels. The shadow of false negatives from predicted incidences (Figure 1, Figure 2, Figure 3, Figure 4, Figure S3, Figure S4 and Figure S5) indicates that a small stochastic component lingers even at our coarse temporal and spatial scales. Not all areas that could potentially be burned do get burnt, because of the dynamics of the interaction of diurnal and nocturnal weather cycles and the spatial patterning of dry fuel, and areas that have been recently burned do not carry fire.

Fuel is a major influence on fire incidence and spread. For example, fires in the Australian desert tend to be most extensive in wet years when fuel builds up to a sufficient amount and continuity to carry fire²⁰. However, it appears that the importance of fuel levels in fire incidence at our spatiotemporal scale is subsumed within our climatic variables, or that spatial heterogeneity in fuel occurs at a finer scale than that of our analysis.

Because ignition of fire by human beings well outweighs ignition of fires by lightning²⁰, the major natural cause, the predominance of climate in estimation is surprising on the surface. However, the accurate estimation of monthly fire incidence from monthly climatic data does not necessarily mean that human beings have little or no influence on fire incidence in Australia in the months of November-February. In temperate Australia, there is active discouragement of ignition, and attempts at suppression after fires are lit, during weather that could result in uncontrollable wildfire. There is less government interference in fire incidence in the tropics and the desert country²⁰. Prevention and suppression in temperate Australia may be having a spatially uniform effect on fire incidence, allowing climate to appear the sole influence. However, for the purpose of estimation of the response of wildfires to climate change, it may be safely assumed that the people of temperate Australia will not relax their vigilance in relation to summer fire, allowing our model to

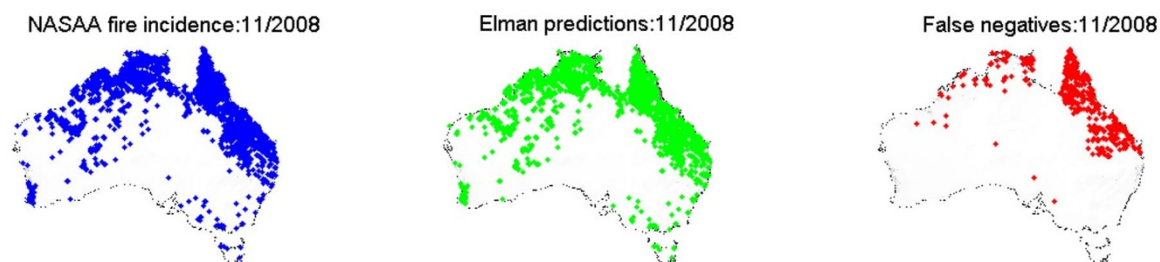


Figure 1 | The NASA fire incidence data, the estimations from the Elman neural network and false negatives from the estimation for November 2008. Maps were generated using MATLAB Software image processing and neural network toolbox. © CSIRO, Australia.



Table 2 | Percentage estimation results and confusion matrix error statistics achieved from the decennium data experiment using the Elman neural network

Time Period	Estimation Accuracy (%)	Sensitivity (%)	Specificity (%)	False Negative (%)	True Negative (%)
Testing 1 {Nov-07}	93.62	97.94	95.22	0.95	96.81
Testing 1 {Dec-07}	91.34	94.5	97.2	1.07	97.8
Testing 1 {Jan-08}	90.78	92.98	93.57	2.32	92.88
Testing 1 {Feb-08}	91.07	95.1	90.87	3.67	95.34
Testing 2 {Nov-08}	94.72	97.32	98.67	0.35	98.56
Testing 2 {Dec-08}	93.45	97.15	95.66	0.78	96.72
Testing 2 {Jan-09}	91.48	95.08	94.17	1.12	94.81
Testing 2 {Feb-09}	92.77	97.1	94.87	1.01	96.14
Testing 3 {Nov-09}	92.59	93.52	94.87	2.55	94.6
Testing 3 {Dec-09}	92.89	95.15	92.06	1.75	92.72
Testing 3 {Jan-10}	90.28	92.11	93.91	4.16	92.44
Testing 3 {Feb-10}	91.33	93.16	90.67	5.01	93.14

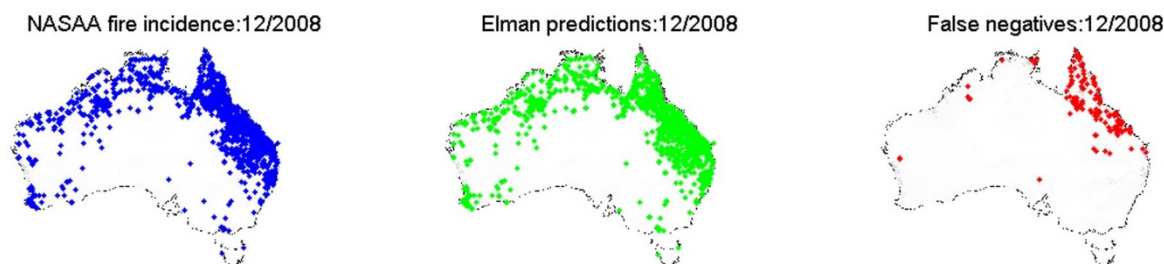


Figure 2 | The NASA fire incidence data, the estimations from the Elman neural network and false negatives from the estimation for the December 2008. Maps were generated using MATLAB Software image processing and neural network toolbox. © CSIRO, Australia.

be used irrespective of the degree of anthropogenic influence, as long as that influence remains uniform within climatic regions.

Methods

An ANN requires an input and a known target for training the system. The training phase modulates the internal layers of the system based on the training inputs. Once the ANN system is trained, it is ready for testing. In the testing phase an ANN produces an output based on all combination of inputs. The Feed Forward Back Propagation, Cascade, Multi-Layer Perception, Time Delay, Recurrent, Radial Basis Function, Elman, Probabilistic, Regression and Learning Vector Quantization networks were applied to the same data sets to establish the best architecture as indicated by estimation accuracy $((TP + TN)/(TP + FN + FP + TN))$ where true positives = TP, true negatives = TN, false positives = FP, false negatives = FN). This was done to establish a comparative generalization capability of the proposed deep²⁴ cognitive imaging system.

The selected Elman network for our deep²⁴ learning mechanism uses a system of ordinary differential equations to model the effects on a neuron of the incoming spike train¹¹.

For a neuron i in the network with action potential y_i the rate of change of activation is given by:

$$\tau_i \dot{y}_i = -y_i + \sigma \left(\sum_{j=1}^n w_{ij} y_j - \theta_j \right) + I_i(t)$$

Where:

τ_i : Time constant of postsynaptic node, y_i : Activation of postsynaptic node, \dot{y}_i : Rate of change of activation of postsynaptic node, w_{ij} : Weight of connection from pre to postsynaptic node, $\sigma(x)$: Sigmoid of x e.g. $\sigma(x) = 1/(1 + e^{-x})$, y_j : Activation of presynaptic node, θ_j : Bias of presynaptic node, $I_i(t)$: Input (if any) to node.

The continuous recurrent neural network is a dynamic systems model of biological neural networks which has been widely used in deep learning mechanism^{24,26,11}. The Elman artificial neural network has typically sigmoid artificial neurons in its hidden layer, and linear artificial neurons in its output layer. In the present study, the MATLAB based design of the Elman network has three primary attributes, namely, “layerdelays” (row vector of increasing 0 or positive delays), “hiddenSizes” (row vector of one or more hidden layer sizes), and “trainFcn” (training function). The best performing Elman network’s “layerdelays” was 1:12, “hiddenSizes” was 135 and “trainFcn” was ‘trainlm’.

We used a gridded matrix of 670 rows and 813 columns for all input data sources. Six data segmentation regions were used for training and testing the network (Figure S1). The segments S1, S2, S4 and S5 have 335 rows and 300 columns. The segments S3 and S6 have 335 rows and 213 columns. The map-based image data (training inputs, testing inputs and training targets) were segmented into six smaller regions to maximize the learning speed while training and optimize the computational memory usage. Six dedicated Elman networks for each of these segments (S1–S6) were trained and tested individually. Final estimation results were constructed by combining the six segmented estimation outputs produced by the six individual networks. We calculated the following values for each of the months: estimation accuracy; sensitivity $(TP / (TP + FN))$; specificity $(TN / (FP + TN))$; where true positives = TP, true negatives = TN, false positives = FP, false negatives = FN.

The main motivation of the present study was to use publicly available climate data sources to establish an effective estimation of continental scale wildfire incidences.

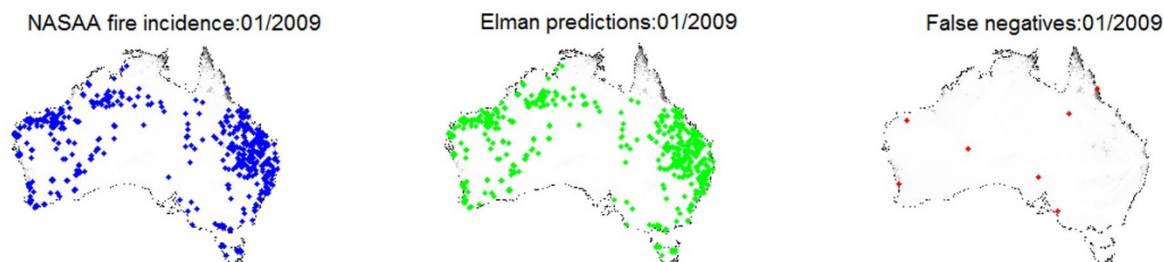


Figure 3 | The NASA fire incidence data, the estimations from the Elman neural network and false negatives from the estimation for the January 2009. Maps were generated using MATLAB Software image processing and neural network toolbox. © CSIRO, Australia.

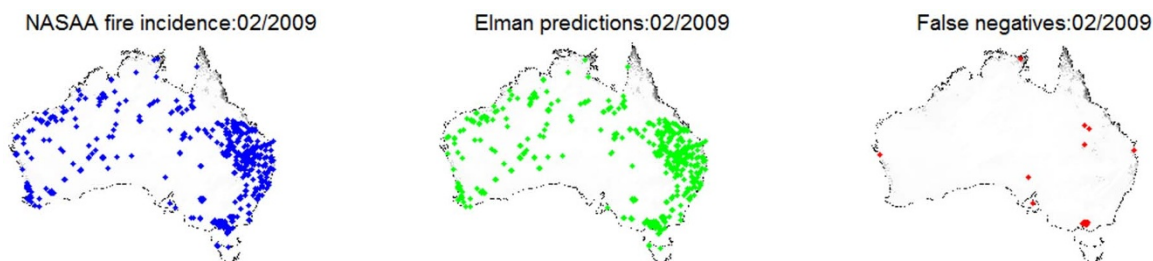


Figure 4 | The NASA fire incidence data, the estimations from the Elman neural network and false negatives from the estimation for the February 2009. Maps were generated using MATLAB Software image processing and neural network toolbox. © CSIRO, Australia.

For the months of November, December, January and February we used the monthly average maps of total evaporation, sensible heat flux, precipitation, incoming solar irradiance, maximum temperature and soil moisture from the Australian Water Availability Project (AWAP²⁸) data base and the monthly average maps of wind speed, vapour pressure and relative humidity from the Australian Bureau of Meteorology (BOM²⁹). Our response variable was based on the data in the monthly Australian bushfire maps from NASA Active (NASAA) fire data (based on satellite images from EOSDIS³⁰). In order to reduce the uncertainties associated with EOSDIS images, latitude-longitude combinations were averaged on 5-km gridded area to calculate representative wildfire locations. Image filtering techniques based on Australian vegetation mask and recorded land usage map were applied to remove the fire locations which were not in native vegetation. Principal components analysis based on singular value decomposition was used to provide least correlated input loadings hence maximum data variance.

Various training and testing data sets were formed from the integrated 10 year long data set comprising data for November, December, January and February, 2001–2010. The Elman method was used to establish the training-testing paradigm which maximized the generalization capability of the neural network architecture. Combinations of % training data and % testing data were varied from {10%–90%} to {50%–50%} to identify the best possible training-testing data balance to achieve maximum estimation accuracy with highest possible sensitivity and specificity. Elman neural network architecture was able to achieve maximum estimation accuracy when 70% of the data were used for training and 30% of the data were used for testing. We therefore used 2001–2007 for training and 2008–2010 for testing. Three training sets were made truly independent from the testing sets as this method provided us with high confidence in the experimental design.

- Bond, W. J. & Keeley, J. E. Fire as a global 'herbivore': the ecology and evolution of flammable ecosystems. *Trends Ecol. Evol.* **20**, 387–394 (2005).
- Bowman, D. M. J. S. *et al.* Fire in the earth system. *Science* **324**, 481–484 (2009).
- Lohman, D. J., Bickford, D. & Sodhi, N. S. Cost of wildfire. *Science* **316**, 376 (2007).
- Gill, A. M. Landscape fires as social disasters: an overview of 'the bushfire problem'. *Glob. Envir. Ch.* **6**, 65–80 (2005).
- Mooney, S. D. *et al.* Late Quaternary fire regimes of Australasia. *Quat. Sci. Rev.* **30**, 28–46 (2011).
- Marlon, J. R. *et al.* Climate and human influences on global biomass burning over the past two millennia. *Nature Geoscience* **1**, 697–702 (2008).
- Boer, M. M., Sadler, R. J., Bradstock, R. A., Gill, A. M. & Grierson, P. F. Spatial scale invariance of southern Australian forest fires mirrors the scaling behaviour of weather events. *Landsc. Ecol.* **23**, 899–913 (2008).
- Spracklen, D. V. *et al.* Impacts of climate change from 2000 to 2050 on wildfire activity and carbonaceous aerosol concentrations in the western United States. *J. Geophys. Res.* **114**, D20301 (2009).
- Westerling, A. L. *et al.* 2011. Continued warming could transform Greater Yellowstone fire regimes by mid-21st century. *PNAS* **108**, 13165–70 (2011).
- Bradstock, R. A., Cohn, J. S., Gill, A. M., Bedward, M. & Lucas, C. Prediction of the probability of large fires in the Sydney region of south-eastern Australia using fire weather. *Intnl. J. Wildland Fire* **18**, 932–943 (2009).
- Elman, J. L. Finding structure in time. *Cognitive Science* **14**, 179–211 (1990).
- Giglio, L., van der Werf, G. R., Randerson, J. T., Collatz, G. J. & Kasibhatla, P. Global estimation of burned area using MODIS active fire observations. *Atmosph. Chem. Phys.* **6**, 957–974 (2006).
- Carmona-Moreno, C. *et al.* Characterizing interannual variations in global fire calendar using data from Earth observing satellites. *Global Change Biology* **11**, 1537–1555 (2005).
- Cary, G., Lindenmayer, D. & Dover, S. *Australia Burning: Fire Ecology, Policy and Management Issues* (CSIRO Publishing, CSIRO submission, Melbourne, 2003).
- Hennessy, K. J. *et al.* *Climate Change Impacts on Fire-Weather in South-East Australia Report C/1061*. (CSIRO Publishing, CSIRO submission, Melbourne, 2006).
- Clarke, H., Lucasc, C. & Smith, P. Changes in Australian fire weather between 1973 and 2010. *Int. J. Climatol.* **33**, 931–944 (2013).
- Byram, G. M. (1959) *Combustion of forest fuels. Forest Fire: Control and Use* pp. 61–89 (McGrawHill Book Co, 1959).

- Goldammer, J. G. & Price, C. Potential impacts of climate change on fire regimes in the tropics based on MAGICC and a GISS GCM-derived lightning model. *Climatic Change* **39**, 273–296 (1998).
- Luke, R. H. *Bushfire control in Australia* (Hodder & Stoughton, 1961).
- Russell-Smith, J. *et al.* Bushfire "down under": patterns and implications of contemporary Australian burning. *Intnl. J. Wildland Fire* **16**, 361–377 (2007).
- McArthur, A. G. *Forest Fire Danger Meter* (Forest Research Institute, Forestry and Timber Bureau, Canberra, Australia, 1973).
- Wilson, R. A. Observations of extinction and marginal burning states in free burning porous fuel beds. *Combust. Sci. Technol.* **44**, 179–193 (1985).
- Parisien, M. & Moritz, M. A. Environmental controls on the distribution of wildfire at multiple spatial scales. *Ecol. Monogr.* **79**, 127–154 (2009).
- Krizhevsky, A., Sutskever, I. & Hinton, G. E. ImageNet Classification with Deep Convolutional Neural Networks. *Advances in Neural Information Processing* **25**, MIT Press, Cambridge, MA.
- Alonso-Betanzosa, A. *et al.* An intelligent system for forest fire risk prediction and fire fighting management in Galicia. *Expert Systems with Applications* **25**, 545–554 (2003).
- Cheng, T. & Wang, J. Integrated spatio-temporal data mining for forest fire prediction. *Trans. GIS* **12**(5), 591–611 (2008).
- Bradstock, R. A. A biogeographic model of fire regimes in Australia: current and future implications. *Glob. Ecol. Biogeogr.* **19**, 145–158 (2010).
- Australian Water Availability Project Website: <http://www.eoc.csiro.au/awap/> (September 2013).
- Australian Bureau of Meteorology web homepage: <http://www.bom.gov.au/> (September 2013).
- The NASA FIRMS MODIS Archive Download service Website: <http://earthdata.nasa.gov/data/near-real-time-data/firms/active-fire-data#tab-content-7> (September 2013).

Acknowledgments

The authors wish to thank the Intelligent Sensing and Systems Laboratory, CSIRO Computational Informatics and the Tasmanian node of the Australian Centre for Broadband Innovation for providing a capability grant that helped to conduct this research. The authors would like to thank Peter Briggs for providing access to the AWAP database. The authors also acknowledge the use of FIRMS data and imagery from the Land Atmosphere Near-real time Capability for EOS (LANCE) system operated by the NASA/GSFC/Earth Science Data and Information System (ESDIS) with funding provided by NASA/HQ.

Author contributions

R.D. and J.A. conceived and designed the experiments. R.D. led development of the cognitive imaging systems and its implementation. J.A. performed NASA-MODIS image and other data processing. A.D. performed data experiments with various neural networks and helped to design optimum network architecture. J.B.K. suggested the research question and wrote a substantial part of the manuscript. R.D., J.A., A.D. also contributed to the writing of the final manuscript.

Additional information

All protocols and methods remain freely available for academic and non-profit research in perpetuity, and supported by the authors published under CC-BY-NC-ND.

Supplementary information accompanies this paper at <http://www.nature.com/scientificreports>

Competing financial interests: The authors declare no competing financial interests.

How to cite this article: Dutta, R., Aryal, J., Das, A. & Kirkpatrick, J.B. Deep Cognitive imaging systems enable estimation of continental-scale fire incidence from climate data. *Sci. Rep.* **3**, 3188; DOI:10.1038/srep03188 (2013).



This work is licensed under a Creative Commons Attribution-NonCommercial-NoDerivs 3.0 Unported license. To view a copy of this license, visit <http://creativecommons.org/licenses/by-nc-nd/3.0>